Diagn Interv Radiol 2024; DOI: 10.4274/dir.2024.242720

PEDIATRIC RADIOLOGY

ORIGINAL ARTICLE

Feasibility study of computed high b-value diffusion-weighted magnetic resonance imaging for pediatric posterior fossa tumors

Semra Delibalta[1]
Barış Genç[2]
Meltem Ceyhan Bilgici[2]
Kerim Aslan[2]

[1]Acıbadem Mehmet Ali Aydınlar University Faculty of Medicine, Atakent Hospital, Department of Radiology, İstanbul, Türkiye

[2]Ondokuz Mayıs University Faculty of Medicine, Department of Radiology, Samsun, Türkiye

PURPOSE

To evaluate the diagnostic efficacy of computed diffusion-weighted imaging (DWI) in pediatric posterior fossa tumors generated using high b-values.

METHODS

We retrospectively performed our study on 32 pediatric patients who had undergone brain magnetic resonance imaging for a posterior fossa tumor between January 2016 and January 2022. The DWIs were evaluated for each patient by two blinded radiologists. The computed DWI (cDWI) was mathematically derived using a mono-exponential model from images with b = 0 and 1,000 s/mm^2 and high b-values of 1,500, 2,000, 3,000, and 5,000 s/mm^2. The posterior fossa tumors were divided into two groups, low grade and high grade, and the tumor/thalamus signal intensity (SI) ratios were compared. The Mann–Whitney U test and receiver operating characteristic (ROC) curves were used to compare the diagnostic performance of the acquired DWI (DWI_{1000}), apparent diffusion coefficient $(ADC)_{1000}$ maps, and cDWI ($cDWI_{1500}$, $cDWI_{2000}$, $cDWI_{3000}$, and $cDWI_{5000}$).

RESULTS

The comparison of the two tumor groups revealed that the tumor/thalamus SI ratio on the DWI_{1000} and cDWI ($cDWI_{1500}$, $cDWI_{2000}$, $cDWI_{3000}$, and $cDWI_{5000}$) was statistically significantly higher in high-grade tumors ($P < 0.001$). In the ROC curve analysis, higher sensitivity and specificity were detected in the $cDWI_{1500}$, $cDWI_{2000}$, $cDWI_{3000}$, and ADC_{1000} maps (100%, 90.90%) compared with the DWI_{1000} (80%, 81.80%). $cDWI_{3000}$ had the highest area under the curve (AUC) value compared with other parameters (AUC: 0.976).

CONCLUSION

cDWI generated using high b-values was successful in differentiating between low-grade and high-grade posterior fossa tumors without increasing imaging time.

CLINICAL SIGNIFICANCE

cDWI created using high b-values can provide additional information about tumor grade in pediatric posterior fossa tumors without requiring additional imaging time.

KEYWORDS

Computed diffusion-weighted imaging, high b-value, magnetic resonance imaging, pediatric posterior fossa tumors, synthetic diffusion-weighted imaging

Corresponding author: Semra Delibalta

E-mail: drsemradelibalta@gmail.com

Received 07 March 2024; revision requested 14 April 2024; last revision received 07 July 2024; accepted 22 July 2024.

Epub: 02.09.2024

Publication date: xx.xx.2024

DOI: 10.4274/dir.2024.242720

Pediatric brain tumors are the most common childhood solid tumors and are frequently located in the posterior fossa.[1,2] The most common tumors in the posterior fossa in children are medulloblastoma (MB), pilocytic astrocytoma (PA), and ependymoma.[3,4]

Although conventional magnetic resonance imaging (MRI) is necessary for the diagnosis of brain tumors and the evaluation of their extent and location, it provides limited information on tumor type and grade.[5] Advanced MRI techniques such as diffusion-weighted imaging (DWI) contribute to the differential diagnosis of these tumors. Diffusion restriction and

You may cite this article as: Delibalta S, Genç B, Ceyhan Bilgici M, Aslan K. Feasibility study of computed high b-value diffusion-weighted magnetic resonance imaging for pediatric posterior fossa tumors. *Diagn Interv Radiol*. 02 September 2024 DOI: 10.4274/dir.2024.242720 [Epub Ahead of Print].

low apparent diffusion coefficient (ADC) values are found more prominently in high-grade tumors with high cellularity than in low-grade tumors.[6] However, when using standard b-values (b = 1,000 s/mm^2), overlaps can be observed in the signal intensity (SI) of high-grade and low-grade tumors.[7,8] When DW images obtained using high b-values (b = 3,000 s/mm^2) and standard b-values in the differential diagnosis of high-grade and low-grade gliomas were compared, more successful results were obtained in examinations with high b-values.[9] However, at a field strength of 1.5T, higher b-values result in low image quality and a low signal-to-noise ratio (SNR).[10,11] Computed DWI (cDWI) is a synthetic DWI mathematically derived from an acquired DWI with two different b-values.[12] Synthetic DWI with high b-values exhibits stronger diffusion effects at a higher SNR than images obtained using existing b-values and can be generated without additional scanning time.[13,14] Studies have demonstrated that cDWI has improved lesion prominence compared with conventional DWI when examining the brain and other body regions.[13,15-19] To the best of our knowledge, no studies have investigated the diagnostic performance of calculated high b-values in pediatric posterior fossa tumors. In the present study, we aimed to evaluate the diagnostic performance of cDWI generated using high b-values in pediatric posterior fossa tumors.

Methods

This study was approved by the Ethics Committee of Ondokuz Mayıs University Faculty of Medicine and was conducted in accordance with the Declaration of Helsinki and Good Clinical Practice guidelines (October 26, 2022, number: 2022/467). The requirement for informed consent was waived.

Main points

- Compared with images generated using existing b-values, synthetic diffusion-weighted imaging (DWI) with high b-values exhibits greater diffusion effects at a higher signal-to-noise ratio and may be produced without additional scanning time.
- The use of computed DWI (cDWI) with high b-values can help distinguish between low-grade and high-grade tumors without requiring more imaging time.
- For differentiating between low-grade and high-grade posterior fossa tumors, $cDWI_{1500}$, $cDWI_{2000}$, and $cDWI_{3000}$ perform better as diagnostic tools than the acquired DWI_{1000} and apparent diffusion coefficient$_{1000}$ maps.

Patients

This study was conducted retrospectively in a single center after approval from the Ethics Committee, and the report was drafted in accordance with the Standards for Reporting of Diagnostic Accuracy Studies guidelines.[20] Between January 2016 and January 2022, 32 pediatric patients who had undergone preoperative brain MRI for posterior fossa tumors and who had not received treatment were included in the study. One patient without a histopathological diagnosis was excluded from the study, and three patients were excluded from the study because artifacts affected the evaluation of the DW images. Finally, 28 patients were included in the study (Figure 1).

Based on the World Health Organization 2021 classification, the patients were divided into two groups: low grade (grade 1 and 2 tumors) and high grade (grade 3 and 4 tumors).[21] The mean age of the low-grade tumor group was 7.5 ± 3.9 years (eight girls: 7 ± 3.4 years; five boys: 8.1 ± 4.0 years), and the mean age of the high-grade tumor group was 9.2 ± 4.3 years (six girls: 9.1 ± 5.1 years; nine boys: 9.2 ± 4.5 years).

Magnetic resonance imaging examination

All examinations were performed using 1.5T MRI (Achieva, Philips Healthcare, Best, Netherlands and Magnetom, SIEMENS AG, Erlangen, Germany) devices. All acquisitions were performed in the multiparametric MRI protocol, using T1WI, T2WI, fluid attenuated inversion recovery, dynamic contrast enhanced MRI, and DWI sequences. The acquisition parameters of the DWI are summarized in Table 1. cDWI was created based on images with b = 0 and 1,000 s/mm^2, with high b-values of 1,500, 2,000, 3,000, and 5,000 s/mm^2, using the mono-exponential model established in a study produced by our team.[14]

Image analysis

Images were evaluated by two radiologists, with evaluations and measurements performed independently of each other's assessment and without knowledge of the tumor pathology. Precontrast T2, precontrast T1, and postcontrast T1WIs were analyzed, and tumor boundaries were established while assessing the cystic, hemorrhagic, and necrotic components of the tumor. Using the volume of interest (VOI) approach and ITK-SNAP, measurements were taken from the solid portion of the tumor using DWI.[22] Similar measurements were calculated manually using ITK-SNAP software from the acquired DWI_{1000}, cDWI (b = 1,500, 2,000, 3,000, and 5000 s/mm^2), and ADC_{1000} maps. In each patient, the tumor and thalamus SI ratio was calculated by measuring the right thalamus using the VOI method.

Statistical analysis

The IBM SPSS (version 22; IBM, Armonk, NY, USA) software program was used in all calculations. The Shapiro–Wilk test was used in all statistical studies to verify normal distribution. Descriptive statistics of the data are presented as n (%), and for normalized variables, mean ± standard deviation values are

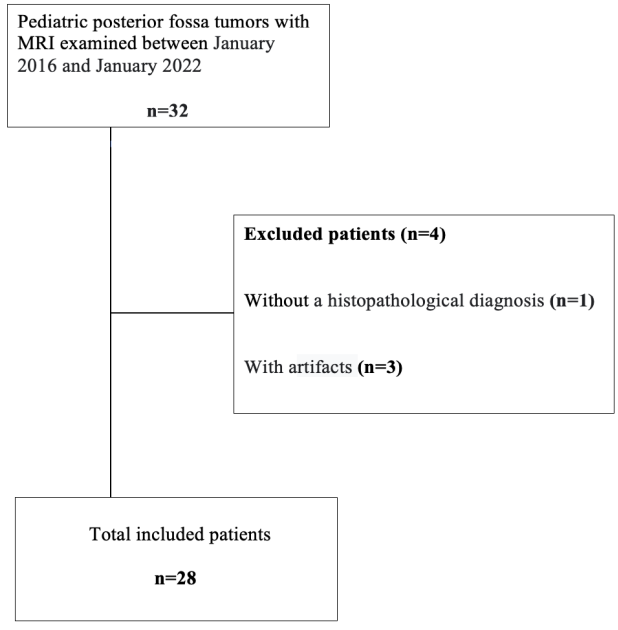

Figure 1. Study flowchart. MRI, magnetic resonance imaging.

provided, whereas for non-normalized variables, the median (min–max) is provided. The Mann–Whitney U test was used for data with normal distribution, comparing the tumor/thalamus SI ratios of high-grade and low-grade tumors on DWI_{1000}, $cDWI_{1500}$, $cDWI_{2000}$, $cDWI_{3000}$, $cDWI_{5000}$, and ADC_{1000} maps. The receiver operating characteristic (ROC) curve was calculated for the diagnostic performance of DWI_{1000}, $cDWI_{1500}$, $cDWI_{2000}$, $cDWI_{3000}$, $cDWI_{5000}$, and ADC_{1000} maps in differentiating high–low grade tumors with the area under the curve (AUC). Youden's index was used to select the optimal predicted probability cut-off. The sensitivity and specificity of the DWI and ADC maps were calculated by determining the cut-off value using an ROC curve analysis. Interobserver correlation was evaluated using the intraclass correlation (ICC) coefficient, and κ values were interpreted as follows: κ = 0.00–0.20, slight agreement; κ = 0.21–0.40, fair agreement; κ = 0.41–0.60, moderate agreement; κ = 0.61–0.80, substantial agreement; and κ = 0.81–1.00, almost perfect agreement.[23] A *P* value <0.05 was considered statistically significant.

Results

In total, 13 low-grade [PA = 7 (54%), posterior fossa ependymoma (grade 2) = 3 (23%), low-grade tumor-diffuse astrocytoma = 3 (23%)] and 15 high-grade [MB = 13 (87%), posterior fossa ependymoma (grade 3) = 1 (1%), glioblastoma = 1 (1%)] tumors were included in our study. The tumor/thalamus SI ratios (median and min–max values) for DWI_{1000}, $cDWI_{1500}$, $cDWI_{2000}$, $cDWI_{3000}$, and $cDWI_{5000}$ in low-grade and high-grade tumors are reported in Table 2. The median (min–max) SI rates were higher in the high-grade tumors than in the low-grade tumors (P < 0.001). When the two tumor groups were compared, the tumor/thalamus SI ratio distributions were more clearly distinguished at higher b-values than at b = 1,000 s/mm^2 (Figure 2). In the ICC test, the kappa value was found to be greater than 0.75 for all parameters, with an almost perfect correlation between 0.82 and 0.95 (*P* < 0.001 for each comparison) (Table 2).

Table 1. Diffusion-weighted imaging sequence parameters

ssEPI DWI b1000		
Parameters	PHILIPS achieva	SIEMENS magnetom
Field of view (mm × mm)	240 × 240	229 × 229
Matrix	192 × 192	192 × 192
Slice thickness	3.50 mm	5 mm
Repetition time	4,200 ms	4,200 ms
Echo time	72 ms	105 ms
Flip angle	90°	90°
Calculated b-values	b1500, b2000, b3000, b5000	b1500, b2000, b3000, b5000

ssEPI, single-shot echo-planar imaging; DWI, diffusion-weighted imaging.

Table 2. Tumor/thalamus signal intensity ratios in diffusion-weighted imaging (DWI) and computed diffusion-weighted imaging at different b-values

Parameters	Low-grade tumors (n = 13) Median (min–max values)	High-grade tumors (n = 15) Median (min–max values)	*P*	ICC (κ values)	*P* (for ICC)
DWI_{1000}	1.09 (0.90–1.71)	1.62 (1.16–2.17)	<0.001	0.82	<0.001
$cDWI_{1500}$	1.00 (0.75–1.70)	1.75 (1.18–2.27)	<0.001	0.89	<0.001
$cDWI_{2000}$	0.82 (0.46–0.70)	1.89 (1.21–2.39)	<0.001	0.91	<0.001
$cDWI_{3000}$	0.59 (0.25–1.69)	1.99 (1.24–2.99)	<0.001	0.94	<0.001
$cDWI_{5000}$	0.38 (0.08–1.66)	2.81 (1.24–6.10)	<0.001	0.95	<0.001

The Mann–Whitney U test was used to compare the tumor/thalamus signal intensity ratios of high-grade and low-grade tumors. The intraclass correlation (ICC) was used to assess interobserver correlation. DWI, diffusion-weighted imaging; cDWI, computed diffusion-weighted imaging.

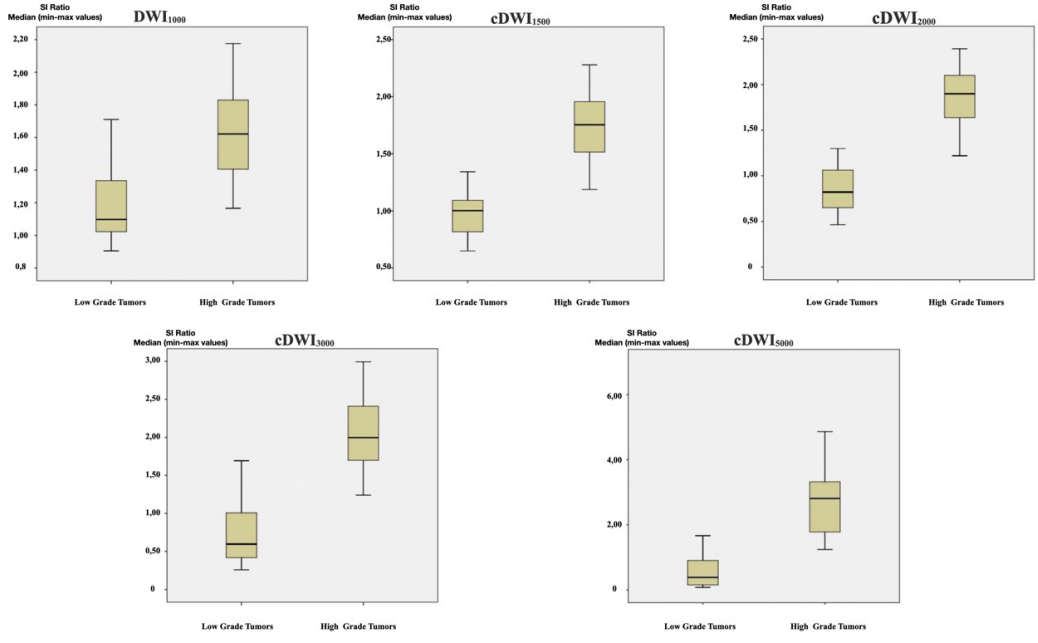

Figure 2. Box plot comparing tumor/thalamus signal intensity ratios in high-grade and low-grade tumors. Compared with diffusion-weighted imaging $(DWI)_{1000}$, the difference between the two groups is more pronounced in computed DWI ($cDWI_{1500}$, $cDWI_{2000}$, $cDWI_{3000}$, and $cDWI_{5000}$). SI, signal intensity.

In the ADC_{1000} maps, median (min–max) ADC values were found to be lower in the high-grade tumors than in the low-grade tumors [low-grade tumor: 1.1 (0.5–1.6) × 10^{-3} mm^2/s; high-grade tumor: 0.8 (0.6–1.0) × 10^{-3} mm^2/s, $P < 0.001$].

In the ROC curve analysis of the DWI_{1000}, cDWI, and ADC_{1000} maps, the AUC values (Figure 3) were found to be statistically significant in all parameters. The AUC value was higher in $cDWI_{3000}$ than in other parameters (AUC: 0.976, $P < 0.001$). In the ROC curve analysis, when optimal cut-off values were used, higher sensitivity and specificity were detected in cDWI (b = 1,500, 2,000, and 3,000 s/mm^2; 100%, 90.9%) than in DWI_{1000} (80%, 81.80%). The ADC_{1000} maps (100%, 90.90%) revealed higher sensitivity and specificity than DWI_{1000} (80%, 81.80%), whereas $cDWI_{5000}$ (93%, 81.80%) displayed higher sensitivity than DWI_{1000} but similar specificity (80%, 81.80%) (Table 3). The DWI_{1000}, cDWI, and ADC_{1000} maps of the two patients diagnosed with juvenile PA and MB are presented in Figures 4 and 5, respectively.

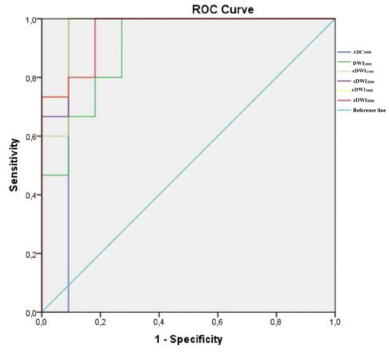

Figure 3. Receiver operating characteristic (ROC) curves at different b-values.

Table 3. Receiver operating characteristic curve analysis results on diffusion-weighted imaging (DWI), computed DWI (cDWI), and apparent diffusion coefficient $(ADC)_{1000}$ maps

Parameters	AUC	Cut-off	Sensitivity(%)	Specificity(%)	*P*
DWI_{1000}	0.903	1.36	80	81.80	<0.001
$cDWI_{1500}$	0.964	1.15	100	90.90	<0.001
$cDWI_{2000}$	0.97	1.15	100	90.90	<0.001
$cDWI_{3000}$	0.976	1.20	100	90.90	<0.001
$cDWI_{5000}$	0.958	1.22	93	81.80	<0.001
ADC_{1000}	0.909	0.00108	100	90.90	<0.001

AUC, area under the curve.

Discussion

In our study, we evaluated the benefits of cDWI created using high b-values for pediatric posterior fossa tumors compared with acquired DWI with standard b-values (b = 1,000 s/mm^2). We determined that the ADC_{1000} maps, DWI_{1000}, $cDWI_{1500}$, $cDWI_{2000}$, $cDWI_{3000}$, and $cDWI_{5000}$ were effective in distinguishing low–high grade tumors. Notably, our study determined that $cDWI_{3000}$ had a higher AUC value for diagnostic performance in the ROC curve analysis than other parameters. As demonstrated in Table 2, as b-values increased, the tumor/thalamus SI ratios decreased in low-grade tumors and increased in high-grade tumors. When compared with images using b = 1,000 s/mm^2, which are frequently used in standard examinations, we observed that the difference between the two groups increased with the increase in b-value. When compared with normal parenchyma areas, with the increase in b-values, a more significant signal reduction was observed in low-grade tumors (Figure 4) and a more pronounced signal in high-grade tumors (Figure 5). As a result, with the increase in b-values, a more significant contrast difference occurred between tumor and normal tissue. In a study using acquired DW images with b = 1,000 and b = 3,000 s/mm^2 on 3T MR to compare low-grade and high-grade differentiation in brain tumors, improved diagnostic performance (high sensitivity and specificity) was demonstrated with higher b-values.[9]

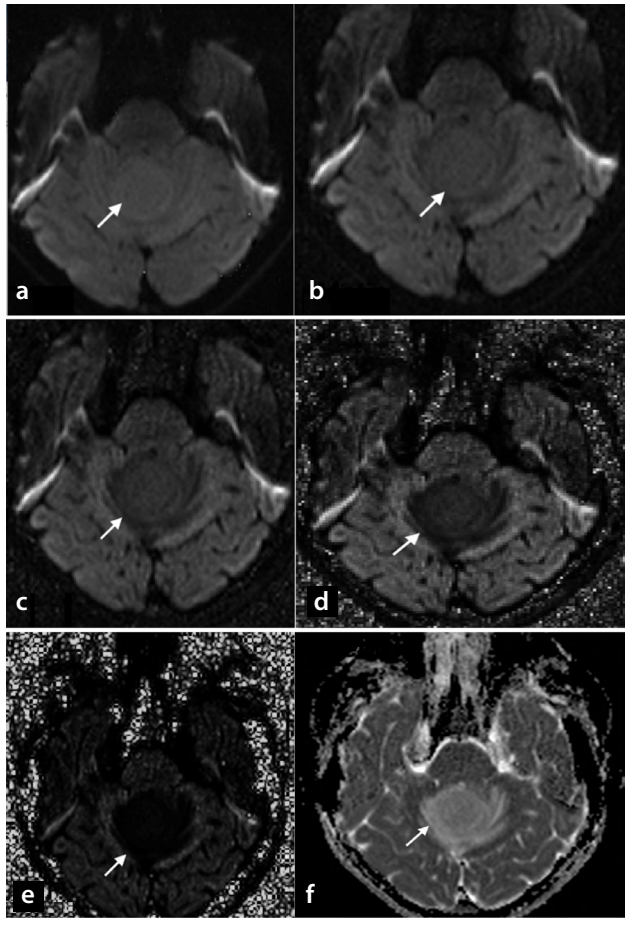

Figure 4. A 15-year-old female with juvenile pilocytic astrocytoma. **(a)** Diffusion-weighted imaging $(DWI)_{1000}$, **(b)** computed DWI $(cDWI)_{1500}$, **(c)** $cDWI_{2000}$, **(d)** $cDWI_{3000}$, **(e)** $cDWI_{5000}$, and **(f)** apparent diffusion coefficient $(ADC)_{1000}$ maps. In the mass located in the 4th ventricle, indicated by the arrow, on DWI with increased b-values, the signal loss of the tumor tissue is more prominent than that of the parenchyma. In addition, a high signal is observed in the parenchyma in the ADC_{1000} maps **(f)**.

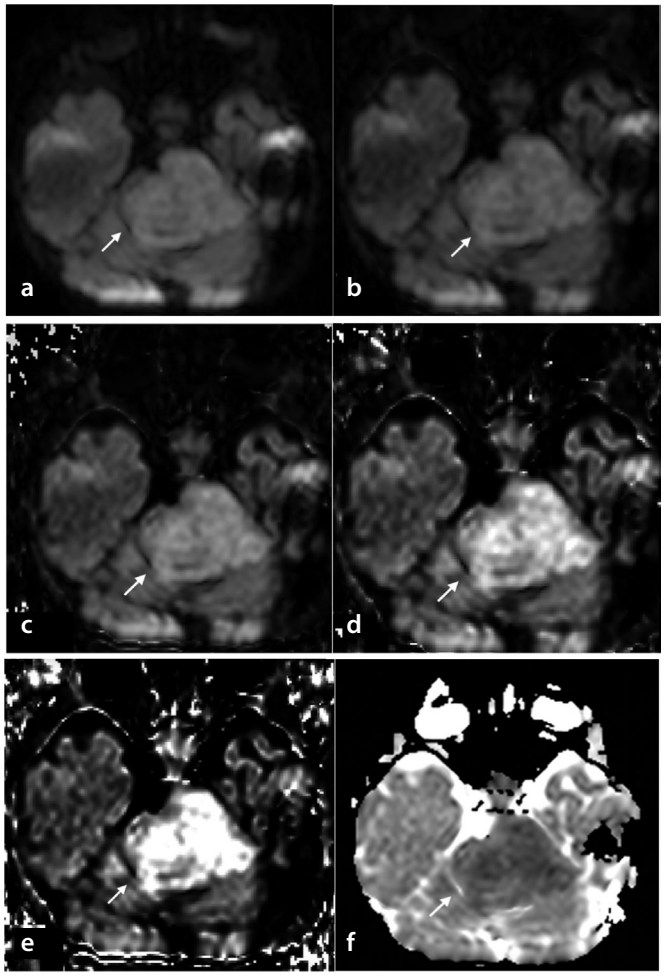

Figure 5. A 13-year-old female with medulloblastoma. **(a)** Diffusion-weighted imaging $(DWI)_{1000}$, **(b)** computed DWI $(cDWI)_{1500}$, **(c)** $cDWI_{2000}$, **(d)** $cDWI_{3000}$, **(e)** $cDWI_{5000}$, and **(f)** apparent diffusion coefficient $(ADC)_{1000}$ maps. In the mass located in the 4th ventricle, indicated by the arrow, as the b-values increase, the signal becomes evident in the tumor tissue, whereas a decrease in the signal is observed in the parenchyma. In addition, a low signal is observed in the parenchyma in the ADC_{1000} maps **(f)**.

In the present study, higher sensitivity and specificity were identified in $cDWI_{1500}$, $cDWI_{2000}$, and $cDWI_{3000}$ compared with DWI_{1000} without increasing acquisition time.

Previous studies on pediatric posterior fossa tumors and gliomas have revealed that high-grade tumors can be effectively distinguished from low-grade tumors with minimal ADC values.[8,24-26] In the present study, the median (min–max) ADC values were found to be lower in high-grade tumors than in low-grade tumors, which is consistent with the literature. In addition, in the present study, in the ROC curve analysis, we determined that $cDWI_{1500}$, $cDWI_{2000}$, and $cDWI_{3000}$ had higher AUC values than ADC_{1000} maps, although $cDWI_{1500}$, $cDWI_{2000}$, and $cDWI_{3000}$ had similar sensitivity and specificity with ADC_{1000} maps (Table 3).

In a study comparing cDWI and acquired DWI in patients with ischemic stroke, $cDWI_{1000}$ and $cDWI_{1500}$ had higher image quality and lesion prominence than acquired DWI_{1000}. However, in the present study, DWI_{2000} and $cDWI_{2500}$ were not found to be an alternative to conventional DWI because of the low lesion detection rates.[15] Kamata et al.[16] reported that $cDWI_{3000}$ was more useful than DWI_{1000} in diagnosing pediatric encephalitis/encephalopathy, and they obtained similar results for acquired DWI_{3000}. In a study investigating synthetic b-values in breast imaging, synthetic images for b1000 and b2000 were obtained and compared with acquired DWI_{850}. The results demonstrated that lesion prominence and image quality were optimal in $cDWI_{1200}$ and $cDWI_{1800}$. In breast imaging, improved lesion visibility and background suppression are theoretically expected with increasing b-values.[13] Similarly, in a study investigating diagnostic sensitivity in breast cancer, $cDWI_{1500}$ was found to be more sensitive than acquired DWI_{1500}.[27] In addition, Daimiel Naranjo et al.[28] revealed that $cDWI_{1200}$ increased the visibility of the tumor without increasing the scanning time, especially in dense breast tissue. In a study on prostate cancer, cDWI with a high b-value was compared with acquired DWI to detect SI differences between cancer and normal tissue, with cDWI identified as more effective. This study verified that cDWI had a better contrast ratio than real images with a high b-value.[29] This study has several limitations. First, it was retrospective and therefore cDWI at high b-values could not be compared with acquired DWI at high b-values. Second, in the literature, measurements have been calculated using region of interest and compared with ADCmin values. We used VOI in our study, which might produce some differences compared with the literature. Third, our study is the first on cDWI in brain tumors, and the results should be verified through further studies.

In conclusion, the present study demonstrated that the diagnostic performance of $cDWI_{1500}$, $cDWI_{2000}$, and $cDWI_{3000}$ is stronger in the differentiation of low-grade and high-grade posterior fossa tumors than that of acquired DWI_{1000} and ADC_{1000} maps. Moreover, the SI ratio between tumor and normal tissue became more pronounced with increasing b-values. Thus, cDWI created with high b-values can contribute to the differential diagnosis of low-grade and high-grade tumors without increasing the imaging time.

Conflict of interest disclosure

Meltem Ceyhan Bilgici, MD, is Section Editor in Diagnostic and Interventional Radiology. She had no involvement in the peer-review of this article and had no access to information regarding its peer-review. Other authors have nothing to disclose.

References

1. Moussalem C, Ftouni L, Abou Mrad Z, et al. Pediatric posterior fossa tumors outcomes: experience in a tertiary care center in the Middle East. *Clin Neurol Neurosurg*. 2020;197:106170. [CrossRef]
2. Paldino MJ, Faerber EN, Poussaint TY. Imaging tumors of the pediatric central nervous system. *Radiol Clin Nort Am*. 2011;49(4):589-616. [CrossRef]
3. Prasad KSV, Ravi D, Pallikonda V, Raman BVS. Clinicopathological study of pediatric posterior fossa tumors. *J Pediatr Neurosci*. 2017;12(3):245. [CrossRef]
4. Bidiwala S, Pittman T. Neural network classification of pediatric posterior fossa tumors using clinical and imaging data. *Pediatr Neurosurg*. 2004;40(1):8-15. [CrossRef]
5. Cha S. Update on brain tumor imaging: from anatomy to physiology. *AJNR Am J Neuroradiol*. 2006;27(3):475-487. [CrossRef]

6. Provenzale JM, Mukundan S, Barboriak DP. Diffusion-weighted and perfusion MR imaging for brain tumor characterization and assessment of treatment response. *Radiology*. 2006;239(3):632-649. [CrossRef]
7. Kono K, Inoue Y, Nakayama K, et al. The role of diffusion-weighted imaging in patients with brain tumors. *AJNR Am J Neuroradiol*. 2001;22(6):1081-1088. [CrossRef]
8. Jaremko JL, Jans LB, Coleman LT, Ditchfield MR. Value and limitations of diffusion-weighted imaging in grading and diagnosis of pediatric posterior fossa tumors. *AJNR Am J Neuroradiol*. 2010;31(9):1613-1616. Erratum in: *AJNR Am J Neuroradiol*. 201;31(10):E90. [CrossRef]
9. Seo HS, Chang KH, Na DG, Kwon BJ, Lee DH. High b-value diffusion (b = 3000 s/mm^2) MR imaging in cerebral gliomas at 3T: visual and quantitative comparisons with b = 1000 s/mm^2. *AJNR Am J Neuroradiol*. 2008;29(3):458-463. [CrossRef]
10. Kim HJ, Choi CG, Lee DH, Lee JH, Kim SJ, Suh DC. High-b-value diffusion-weighted MR imaging of hyperacute ischemic stroke at 1.5T. *AJNR Am J Neuroradiol*. 2005;26(2):208-215. [CrossRef]
11. Meyer JR, Gutierrez A, Mock B, et al. High-b-value diffusion-weighted MR imaging of suspected brain infarction. *AJNR Am J Neuroradiol*. 2000;21(10):1821-1829. [CrossRef]
12. Blackledge MD, Leach MO, Collins DJ, Koh DM. Computed diffusion-weighted MR imaging may improve tumor detection. *Radiology*. 2011;261(2):573-581. [CrossRef]
13. Bickel H, Polanec SH, Wengert G, et al. Diffusion-weighted MRI of breast cancer: improved lesion visibility and image quality using synthetic b-values. *J Mag Reson Imaging*. 2019;50(6):1754-1761. [CrossRef]
14. Higaki T, Nakamura Y, Tatsugami F, et al. Introduction to the technical aspects of computed diffusion-weighted imaging for radiologists. *Radiographics*. 2018;38(4):1131-1144. [CrossRef]
15. Sartoretti T, Sartoretti E, Wyss M, et al. Diffusion-weighted MRI of ischemic stroke at 3T: value of synthetic b-values. *Br J Radiol*. 2021;94(1121):20200869. [CrossRef]
16. Kamata Y, Shinohara Y, Kuya K, et al. Computed diffusion-weighted imaging for acute pediatric encephalitis/encephalopathy. *Acta radiol*. 2019;60(10):1341-1347. [CrossRef]
17. Fukukura Y, Kumagae Y, Hakamada H, et al. Computed diffusion-weighted MR imaging for visualization of pancreatic adenocarcinoma: comparison with acquired diffusion-weighted imaging. *Eur J Radiol*. 2017;95:39-45. [CrossRef]
18. Takeuchi M, Matsuzaki K, Harada M. Computed diffusion-weighted imaging for differentiating decidualized endometrioma from ovarian cancer. *Eur J Radiol*. 2016;85(5):1016-1019. [CrossRef]
19. Jendoubi S, Wagner M, Montagne S, et al. MRI for prostate cancer: can computed high b-value DWI replace native acquisitions? *Eur Radiol*. 2019;29(10):5197-5204. [CrossRef]
20. Cohen JF, Korevaar DA, Altman DG, et al. STARD 2015 guidelines for reporting diagnostic accuracy studies: explanation and elaboration. *BMJ Open*. 2016;6(11):e012799. [CrossRef]
21. Louis DN, Perry A, Wesseling P, et al. The 2021 WHO classification of tumors of the central nervous system: a summary. *Neuro Oncol*. 2021;23(8):1231-1251. [CrossRef]
22. Yushkevich PA, Pashchinskiy A, Oguz I, et al. User-guided segmentation of multi-modality medical imaging datasets with ITK-SNAP. *Neuroinformatics*. 2019;17(1):83-102. [CrossRef]
23. Landis JR, Koch GG. The measurement of observer agreement for categorical data. *Biometrics*. 1977;33:159-174. [CrossRef]
24. Rumboldt Z, Camacho DL, Lake D, Welsh CT, Castillo M. Apparent diffusion coefficients for differentiation of cerebellar tumors in children. *AJNR Am J Neuroradiol.* 2006;27(6):1362-1369. [CrossRef]
25. Lee EJ, Lee SK, Agid R, Bae JM, Keller A, Terbrugge K. Preoperative grading of presumptive low-grade astrocytomas on MR imaging: diagnostic value of minimum apparent diffusion coefficient. *AJNR Am J Neuroradiol*. 2008;29(10):1872-1877. [CrossRef]
26. Chen Z, Ma L, Lou X, Zhou Z. Diagnostic value of minimum apparent diffusion coefficient values in prediction of neuroepithelial tumor grading. *J Magn Reson Imaging*. 2010;31(6):1331-1338. [CrossRef]
27. Park JH, Yun B, Jang M, et al. Comparison of the diagnostic performance of synthetic versus acquired high b-Value (1500 s/mm2) diffusion-weighted MRI in women with breast cancers. *J Magn Reson Imaging*. 2019;49(3):857-863. [CrossRef]
28. Daimiel Naranjo I, Lo Gullo R, Saccarelli C, et al. Diagnostic value of diffusion-weighted imaging with synthetic b-values in breast tumors: comparison with dynamic contrast-enhanced and multiparametric MRI. *Eur Radiol*. 2021;31(1):356-367. [CrossRef]
29. Ueno Y, Takahashi S, Ohno Y, et al. Computed diffusion-weighted MRI for prostate cancer detection: the influence of the combinations of b-values. *Br J Radiol*. 2015;88(1048):20140738. [CrossRef]